Marine Geology 494 (2026) 107733

Contents lists available at ScienceDirect

Marine Geology

journal homepage: www.elsevier.com/locate/margo

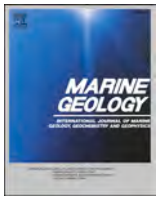

Research Article

A morphological upscaling approach to modelling patterns of long term shoreface change and their synoptic climate drivers in Southeast Australia

T.R. Mortlock [a,b,*], I.D. Goodwin [a,b], M. Ribó [a,c]

[a] School of Natural Sciences, Macquarie University, Sydney, New South Wales 2109, Australia
[b] Climate Change Research Centre, University of New South Wales, Sydney, New South Wales 2052, Australia
[c] School of Science, Auckland University of Technology, Auckland, New Zealand

ARTICLE INFO

Keywords:
Wave climate
Sediment transport
Shoreface
Coastal morphology
Coastal modelling
Coastal storms

ABSTRACT

This study presents a novel method to determine the long-term morphological response of the lower shoreface to regional climate forcing on wave-dominated coasts. By integrating synoptic wave climate typing, coupled wave-hydrodynamic-sediment transport modelling, and frequency-based morphological upscaling, the approach is evaluated using a rare, centennial-scale bathymetric dataset from Byron Bay, in Eastern Australia. Application to eight sites along the Southeast Australian coast, with detailed analysis at two erosion hotspots, suggests that the 30 to 35-m depth zone is the ultimate seaward limit of significant centennial-scale sediment transport under extreme storm conditions. This boundary has implications for both the design of coastal infrastructure, and the extraction of offshore sand. The study also demonstrates that only storms from directions normal to the coast can induce significant sediment transport on the lower shoreface, while storms clockwise of southeast are too oblique to facilitate long-term cross-shoreface transport. Results also indicate that the lower shoreface, like the upper shoreface on event timescales, can rotate in response to directional wave climate forcing on centennial timescales.

1. Introduction

Storm wave events are the principal agent of episodic erosion of the subaerial beach and foredunes on wave-dominated sandy coasts [Vos et al., 2023], but their role in redistributing sand from the lower to upper shoreface over long timescales is poorly understood. Because of the low volumetric rate and frequency of storm-driven onshore transport [Kinsela et al., 2016], this cross-shelf input is usually not included in sediment budget analyses of coastal compartments [Rosati, 2005].

When integrated over decades to millennia, however, even a low rate of onshore supply may offset the offshore transport and shoreline recession generally expected of beaches responding to rising sea levels [Rosati et al., 2013; Patterson and Nielsen, 2016]. The location and ultimate seaward depth at which a low-frequency onshore feed may occur is also important for beach nourishment schemes. Beach nourishment from offshore sources is considered a cost-effective way to maintain beach widths along erosive shorelines, but offshore dredging should not deplete beaches of sand that otherwise would be moving landward over the long term.

In a continental shelf environment, sand transport does not occur all the time and usually takes place during episodic resuspension events [Harris and Wiberg, *2002*]. There are several processes that can lead to sand transport outside the surf zone, including geostrophic currents, density cascading, internal and coastal-trapped waves, surface wind shear, infra-gravity waves and gravity waves. Navier-Stokes theory indicates that in the shoaling zone (from the seaward edge of the surf zone to wave base), gravity wave-driven currents are at least an order of magnitude greater than those produced by other processes. Velocity skewness and asymmetry in the shoaling wave profile means the direction of wave-driven transport outside the surf zone is almost always onshore-directed [O'Donoghue and Wright, 2004; Ruessink et al., 2011]. It follows, therefore, that storm wave events provide the primary mechanism for an episodic, onshore sand feed from deeper water, assuming a ready supply.

Observations of this long-term process, however, are scarce because the magnitude of change during a single storm event is so small that it is beyond the limits of measurement. The only observations of lower shoreface change are from repeat surveys separated hundreds of years apart. Goodwin et al. [2013] digitized a lead-line survey from 1883 at Byron Bay on the far north coast of New South Wales (NSW), Australia,

* Corresponding author at: School of Natural Sciences, Macquarie University, Sydney, New South Wales 2109, Australia.
E-mail address: t.mortlock@unsw.edu.au (T.R. Mortlock).

https://doi.org/10.1016/j.margeo.2026.107733
Received 24 June 2025; Received in revised form 6 February 2026; Accepted 10 February 2026
Available online 14 February 2026

and compared it to a bathymetric Lidar survey of the area in 2011 to determine centennial-scale seabed depth changes. Byron Bay is located at the most-easterly point of the Australian coast and is exposed to moderate wave energy from the tropics through to the mid-latitudes. Goodwin et al. [2013] found that over 128 years, there was cumulative bed elevation change of up to 2.5 m in water depths from 10 to 25 m, and up to 1.5 m out to the 40-m isobath. This equates to less than one centimetre of change per storm on the lower shoreface (assuming an average of three storms per year, as the local wave climate suggests).

In the absence of centennial-scale observations, the sedimentological shoreface response to persistent atmospheric and wave climate regimes needs to be investigated from a modelling perspective. Most long-term coastal evolution studies are based on geomorphological models [Cowell et al., 1995; Daley, 2011] that describe the shoreward translation of sections of the cross-shelf profile that are 'misfit' with present-day sea level. The premise is that sand deposits on the shelf, relict from previous episodes of low sea-level, produce a dis-equilibrium stress that is re-equilibrated across the shelf profile as a lagged response to sea-level rise. While these models provide a useful conceptual framework, the main variables controlling transport are shelf slope and sea-level. They provide little information on the physical processes responsible for shelf sand transport.

Process-based morphological models, instead, try to integrate all major physical processes into the simulation of sand transport. However, they often become computationally impractical (and physically unstable) when applied over longer time scales. To circumnavigate these issues, some novelty in experiment design is required.

Several morphological evolution techniques have been used to speed-up medium-term modelling (months to years) [Cowell et al., 1995; Roelvink, 2006; Ranasinghe et al., 2011], aiming to circuit-break the feedback between waves, currents, and morphology at each time step. The "MORFAC" (Morphological Acceleration Factor) approach involves increasing the modelled bed change by applying a scaling factor to the sediment continuity equation, effectively speeding up the simulated time scale [Li, 2010]. However, for long-term applications (decades to millennia), simply scaling timeseries results can still render computation times prohibitively long. For certain applications, it also means timesteps that have no significant impact on the net outcome are still being included in the modelling process.

To model truly long-term (i.e., centennial-scale) transport with process-based models, a more efficient method may be to capture the range of episodic transport events in detail, and then upscale the morphological response based on a probability of occurrence scalar. The assumption is that all change in shallow water reduces to a long-term equilibrium in line with the modal (non-storm) wave climate, while morphological change outside (seaward of) the surf zone is the integral of storm wave events over the long term.

Under this premise, only the high energy storm wave climate needs to be modelled as the primary agent of infrequent, episodic, lower shoreface transport events, with all intermediate non-storm (modal) wave conditions only relevant for shallow water, upper shoreface change. In this way, a process-based model can be used to look at centennial-scale, lower shoreface sediment transport under directionally discrete atmospheric and wave climate forcing.

In the Southern Hemisphere, the east coasts of South Africa, Australia and South America experience similar wave climates and include storm wave events that are the product of ex-tropical cyclones, subtropical cyclones and extra-tropical cyclones, known as East Coast Lows (ECLs) (Browning and Goodwin, 2013). ECLs are a common feature across the Southern Hemisphere extra-tropics, for example, in Brazil [Evans and Braun, 2012], and South Africa [Taljaard, 1995], forming in late Austral autumn to winter. The east coast of Australia is particularly impacted by the frequency and intensity of ECL storm wave climate since these storms are concentrated in the Tasman Sea. The impact of ECLs on sand transport, however, needs to consider the influence of wave direction (storm track) as well as wave height, as evidenced by the deceptively destructive ECL in June 2016 along the southeast Australian coast [Mortlock et al., 2017].

Browning and Goodwin [2013] identified three types of storms along the Southeast Australian Shelf (SEAS), based on cyclogenesis and track. These include (i) poleward-moving tropical cyclones or tropical lows in the Coral Sea, producing north-east to easterly (NE-E) storm wave conditions along the shelf, (ii) ECLs of both subtropical and extratropical origin in the Tasman Sea, producing east to south-easterly (*E*-SE) storm waves, and (iii) extratropical lows cut off from the circumpolar trough in the Southern Tasman Sea and Southern Ocean, producing south-east to southerly (SE-S) storm waves (Fig. 1).

Here we propose a method for linking different shoreface sediment transport patterns to wave climate drivers by combining synoptic wave climate typing, morphological upscaling and physics-based modelling. We use the storm wave type classification of Browning and Goodwin [2013] and Mortlock and Goodwin [2015] with a coastal morphological model to examine the shoreface transport pattern of each storm type along the SEAS. We then use the frequency of occurrence of these storm wave types as observed from wave buoy records to upscale the seabed change pattern of each storm type to estimate the cumulative shoreface response at locations across the SEAS. The concept of morphologically upscaled climate-linked patterns of shoreface change was first introduced in Goodwin et al. [2020], with this present paper applying and evaluating the concept for the first time. Whilst the focus of this paper is on south-east Australia, the methods, results and conclusions are widely applicable to passive margin coasts with gentle sloping continental shelves such as the east coasts of South Africa, Australia and South America between 25° S and 45°S latitudes, where an equatorward regional longshore sand transport system occurs. The results are particularly important for micro to meso-tidal coasts where wave dominance occurs and there is minimal fluvial sediment discharge to the littoral zone. In this case, the net sediment transport in river entrances and estuaries is landward over the Holocene.

2. Study sites

Two regional coastal models were set up along the SEAS – one covering the Sydney and central NSW coast and shelf, and a second covering the north NSW coast and shelf. Within these two regional domains, three sites were modelled in high resolution: 1) Collaroy-Narrabeen, a headland-bay beach on Sydney's Northern Beaches, 2) Terrigal-Wamberal, also a headland bay-beach on the central coast of NSW, and 3) Byron Bay, an open longshore transport coast on the north coast of NSW. These sites have all been identified as 'erosion hotspots' by NSW State Government [Office of Environment and Heritage, 2017], largely due to inappropriate historical development within the active coastal planform, resulting in a significant number of properties at risk of current and future coastal hazards. Moreover, they benefit from long-term, directional wave buoy records in proximity, and high-resolution local bathymetry and seabed mapping.

2.1. Collaroy-Narrabeen

Collaroy-Narrabeen (33°S, 151°E) (location Fig. 1), hereafter 'Narrabeen', is a swash-aligned embayed beach facing east, approximately 4 km in length, and located 20 km north-east of the Sydney CBD on Sydney's populous northern beaches. The bay is afforded significant shadowing from southerly wave energy by Long Reef headland, to the south. However, it has a long history of erosion problems in part caused by a legacy of development into the active beach zone. It is considered a closed compartment in terms of the upper shoreface sediment budget, with rock headlands and reefs to the north and south preventing an alongshore exchange of sand. The shoreface slope is steep (upper shoreface approximately 2.2%, lower shoreface 1.4%) and complex, comprising a series of shore-normal rock reef platforms and fine to coarse-grained quartz sands [Ribó et al., 2020].

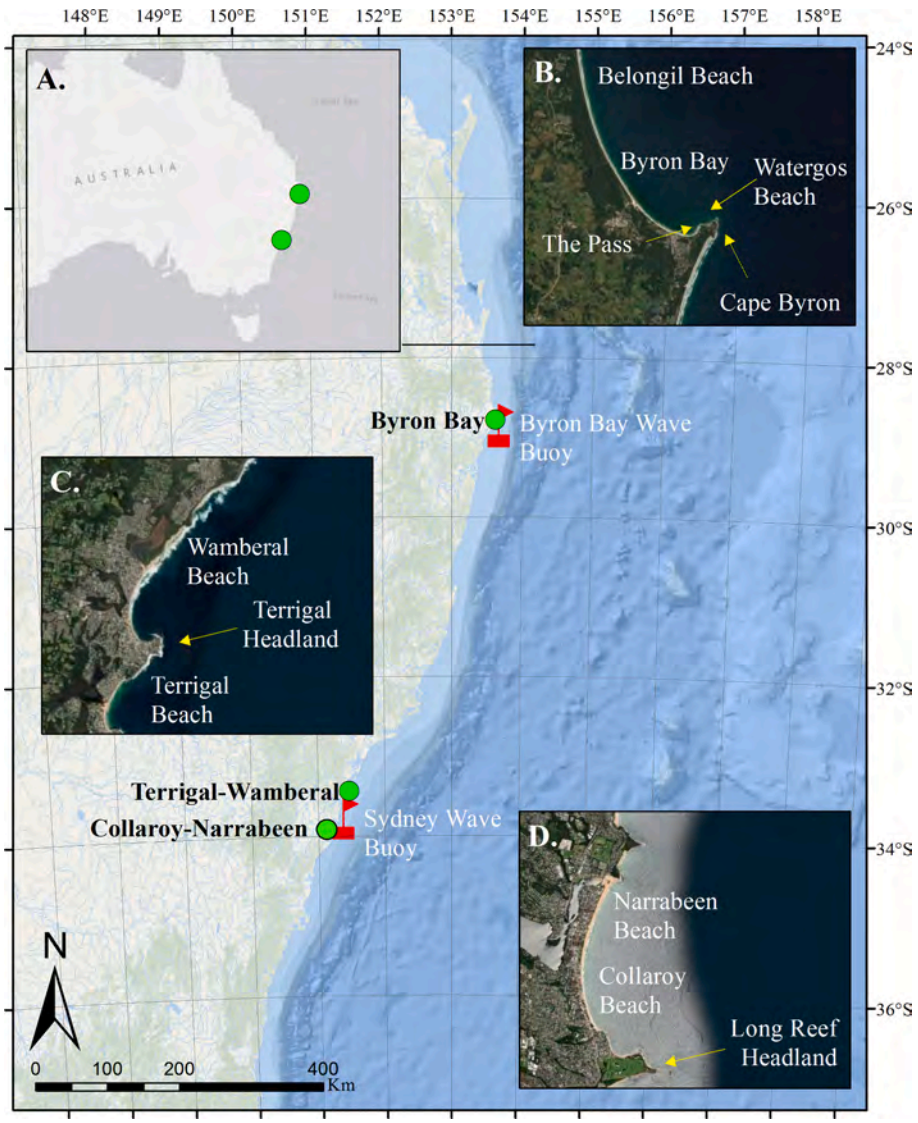

Fig. 1. Map showing the Southeast Australian coast (main image) with the three study sites (green circles) and two wave buoys (red flags). Inset A shows the location of the study sites relative to the rest of Australia. B shows the Byron Bay modelled area; C shows the Terrigal-Wamberal modelled area and D shows the Collaroy-Narrabeen modelled area. (For interpretation of the references to colour in this figure legend, the reader is referred to the web version of this article.)

2.2. *Terrigal-Wamberal*

Terrigal-Wamberal (33°S, 151°E) (location Fig. 1), hereafter 'Wamberal', is a swash-aligned headland-bay beach facing south-east, approximately 4 km in length, located 50 km north-east of the Sydney CBD on the densely-populated NSW central coast. The bay is situated to the north of Terrigal headland. It has a similar shoreface slope and composition as Narrabeen, and monitoring at both sites suggests synchronous erosion/accretion trends [Bracs et al., 2016]. The south-easterly aspect and smaller southern headland, however, means it experiences less shadowing from southerly wave energy than Narrabeen. Wamberal also experiences ongoing erosion problems related to development into the active beach zone.

2.3. *Byron Bay*

Byron Bay (29°S, 154°E) (location Fig. 1) is a headland-bay beach facing north-east, approximately 6 km in length, located 40 km south of the NSW / Queensland state border. The bay extends north of Cape Byron, the most easterly point on the Australian mainland, to Belongil Creek, encompassing Wategos Beach, The Pass, Main Beach and Belongil Beach. Belongil Beach, in particular, has a long history of erosion problems purportedly exacerbated by coastal infrastructure. The shoreface slope is shallower than at Wamberal and Narrabeen (upper shoreface approximately 1.9%, lower shoreface 0.6%), and comprises mainly fine-to-medium grained quartz sands with very few exposed rock reefs [Ribó et al., 2020]. A group of small uninhabited islets called Julian Rocks are located approximately 4 km offshore and impact the wave refractional pattern during east and north-east wave conditions.

In Supplementary Information, we also provide modelling results that were undertaken for additional locations along the SEAS, including Moruya, Batemans Bay, Palm Beach, Hat Head, Smoky Cape, and Scotts Head. However, for the sake of brevity and for the purpose of demonstrating the validity of this approach, only results at Byron Bay, Wamberal and Narrabeen are analysed here.

3. Datasets

3.1. *Instrumental wave data*

Along the moderate wave energy SEAS, instrumental wave data have been collected since the mid-1970s when the New South Wales (NSW)

government commenced wave monitoring. Wave data are available for seven mid-shelf locations at (south to north) Eden, Batemans Bay, Port Kembla, Sydney, Crowdy Head, Coffs Harbour and Byron Bay. This data set provides observational coverage of approximately 1000 km of mid-shelf waves (60–100 m depth) along the western boundary of the Tasman Sea.

In this study, wave data from the Sydney and Byron Bay buoys were used to generate synthetic storm wave conditions at the study sites. While all buoys along the SEAS are now directional, these are the only two sites to have long-term directional wave information from which to derive robust directional extreme values (Table 1). The locations of these buoys in relation to the study sites is shown in Fig. 1.

Both buoys measure hourly wave spectra, from which parametric data are derived. In this paper we use the one-hourly significant wave height, H_s (m), wave period at the primary spectral peak, T_p (s), and mean wave direction, *MWD* (degrees True North, ° TN), to describe storm wave characteristics. Although most modal wave conditions are likely to be deep-water waves at the buoy locations (where water depth is greater than half the wavelength, $d > L/2$), this condition is not always satisfied for storm waves traveling at periods of 10 s or more. This study therefore deals with a mid-shelf, intermediate-to-deepwater storm wave climatology.

3.2. Hindcast wind data

There is no operational ocean wind observation network along the SEAS. Instead, reanalysis winds were used to provide a wind field to accompany the storm wave forcing. We used the National Center for Environmental Prediction's Climate Forecast System Reanalysis (NCEP CFSR) and CFSRv2 wind data [described in Saha et al., 2010]. This was preferred over other available reanalyses because (i) it has proven to be a reliable product for driving wave hindcasts in this region [Cardno, 2012; Durrant et al., 2014], and (ii) it is available on a high spatial and temporal grid (0.3°, hourly from 1979 to present).

Hourly u and v wind components were extracted at the nearest grid cell to the Sydney and Byron Bay wave buoys over the period of directional wave observations. In each case, the nearest output point was ~0.01° (1.5 km) away from the real buoy mooring location.

Most reanalysis winds, including CFSR, are known to exhibit a negative bias at higher velocities [Stopa and Cheung, 2014], particularly near the coast. This can contribute to an under-estimation of near-coast storm wave heights in wave hindcasts driven by reanalysis winds [Durrant et al., 2014]. Cardno [2012] found that by applying a scaling factor to CFSR near-coast winds along the SEAS, modelled storm wave heights from a WaveWatch III model (driven by the up-scaled near-coast winds) better matched observations.

The upscaling was applied linearly along the shelf, based on distance from the coast. Wind speeds were increased by 5% from 60 to 100 km offshore, by 10% between 30 and 60 km, and by 20% within 30 km of the coast. As both wave buoys are located within 30 km of the coast, CFSR wind speeds were increased by 20% at all of the study sites with the aim of better replicating storm wave conditions in the modelling.

3.3. Bathymetric data

The seabed topography in the models comprised a mosaic of best-available bathymetries covering the shoreface (in this case, the shoreline to the 60 m isobath). The 250-m bathymetry and topography grid of Australia (AusBathy) [Whiteway, 2009] was the baseline data for the regional domains. From approximately the 40 m isobath to the coast, AusBathy was largely replaced by a number of multi- and single-beam echosounder surveys (MBES, SBES) and marine lidar data, undertaken and/or commissioned by NSW Office of Environment and Heritage (OEH). MBES and lidar data were gridded to 5-m2 resolution, while most SBES surveys comprised a series of shore-normal transects at 25 or 50-m spacing.

The mosaiced data were interpolated to the model mesh using the nearest neighbour algorithm. Several iterations with varying buffers were required to ensure a smooth transition between AusBathy and adjacent data.

Table 1
Directional buoy records at Sydney and Byron Bay. Water depths reflect current moored position.

Wave buoy	Latitude	Water depth (m)	Directional buoy deployed
Sydney	−33.77	92 m	3 Mar 1992
Byron Bay	−28.85	62 m	26 Oct 1999

3.4. Seabed characterisation and grain size information

Seabed substrate types, locations and grain size information were derived from a large number of mapping and sampling studies compiled in Ribó et al. [2020]. This information was used to apply variable bottom roughness, bed friction and erodible bed depths in the modelling.

4. Experiment design

4.1. Conceptual process

To investigate patterns of shoreface response, we first decomposed the primary drivers (extreme waves and winds) into component parts and sampled a range of storm conditions conducive to episodic transport. The wind and wave scenarios were then refracted across the shelf to estimate the morphological response over the shoreface, and then a morphological upscaling factor was used to express results in terms of the centennial-scale transport patterns.

The storm wave scenarios are based on the directional observational buoy records back to the 1990s. An understanding of these scenarios in a historical context, especially their correlation to Pacific decadal variability phases, and El Nino Southern Oscillation phases, has been extended through the work of Browning and Goodwin [2013], and Goodwin et al. [2016]. The relevance of the buoy records has been evaluated against hindcast products. The past century has contained a mixture of decadal to multi-decadal variability that was typically of the past millennium (Goodwin, 2025). Our upscaling approach does not include potential shifts in storm wave climate over the next 100 years because model projections are inconclusive due to difficulty in modelling east coast weather regime changes. There is some indication that the storm wave events may be less frequent but more intense, but it is not conclusive and relies on the potential changes in the South Pacific Split Jet strength. Instead, our approach takes the form on a Causal Network Approach providing empirical risk-based scenarios, see Goodwin [2025] and Shepherd et al. *[2018]*, [Shepherd, 2019], [Shepherd, 2021].

4.2. Wind and wave scenarios

The wave climate was deconstructed based on height and direction criteria. We sampled two different energy levels which we refer to as “moderate” and “high” energy storm conditions. Each energy level was split into three directional groups (NE to E, E to SE and SE to S) to investigate the influence of wave direction on sand transport. In total, six wave and wind scenarios were used (Table 2).

Table 2
Storm wave and wind scenarios used in this study.

Energy level	Directional group		
	NE – E (< 100°)	E – SE (100–145°)	SE – S (> 145°)
High-energy storms	1	2	3
Moderate-energy storms	4	5	6

The approach of using synthetic storms derived from a probabilistic assessment of observed storm parameters has long been used within the coastal engineering literature for assessing modelled "design" storm conditions and impacts (e.g. *Clauss* et al. [1997]; You and Lord [2008]; Shand et al. [2011]; Soldevilla et al., [2015]). The approach is attractive in that it discretises a complex storm wave climate into an idealised set of conditions that produce an understandable modelled impact. Over centennial timescales, it also avoids the impossibility of modelling every storm event in detail. However, in adopting this approach, the transient nature of storms, and the consequential change in storm wave direction and impacts on sediment transport as the storm moves, is not included.

To construct the storm scenarios, we first identified storm wave events in the buoy record using the Peaks Over Threshold (POT) method [Goda, 2010]. Two sets of conditions were used. The first was a threshold H_s of 2 m for events that lasted at least 72 h, with a minimum interval of 24 h between storm events. These were designed to identify extra-tropical storms which are typically lower energy but longer duration than those of tropical-origin. The second POT used a higher threshold H_s of 3 m, with a minimum storm duration of 6 h. This identified higher energy, more transient storms such as Tropical Lows or Ex-Tropical Cyclones. This returned an average annual storm frequency of 14 across all buoys (from 11 at Eden to 16 at Sydney), which is similar to results obtained by previous authors [You and Lord, *2008*; Shand et al., 2011].

'High-energy' synthetic storm events were constructed using the 95th percentile peak storm wave height of all identified historical storms. 'Moderate-energy' storms were constructed using the 50th percentile peak storm wave height of all identified historical storms.

We did not extrapolate to storm conditions beyond the buoy record length because the cumulative impact of these storms on cross-shelf transport is limited by their rarity. While very high energy events can have lasting impacts for the subaerial beach and dunes, it is the cumulative effect of moderate- to high-energy storm wave events, with sufficient wave base and energy to transport sand across the shelf but with sufficient frequency that their effect becomes significant when integrated over long time scales, that are most likely to provide the mechanism for cross-shelf transport.

4.3. Directional wave separation

Storm events were separated into three directional sectors (NE – E, E – SE, SE – S) to investigate the influence of wave directionality and climate forcing on shoreface transport. The NE – E group included storms with a mean direction <100°; the E – SE group between 100 and 140°; and the SE – S group included all those >140°. The directional cut-offs were located iteratively by comparing the synoptic patterns produced by each group to those identified in Browning and Goodwin [2013]. The synoptic patterns for each group are shown in Fig. 2.

The climate patterns shown in Fig. 2 represent the composite anomalies of all sea level pressure (SLP) configurations at the time of peak-storm wave conditions for each storm event identified within the respective directional sector. In all cases, the composites were subtracted from the long-term mean to show the anomalous pattern.

Fig. 2 shows that storm wave events from the NE – E are generated from a low-pressure trough extending over Southeast Australia into the Coral Sea and interacting with intensified anticyclones in the Tasman Sea. Storm wave events from the E – SE result from a more meridional interaction between a low-pressure cell in the Coral to North Tasman Seas and a blocking high-pressure system, to the south, in the Southern Tasman Sea. Storm wave events from the SE – S result from a low-pressure cell in the Central Tasman Sea and an intense high-pressure system over Southeast Australia and the Southern Ocean. These patterns conform to the synoptic storm types identified by Browning and Goodwin [2013] and Goodwin et al. [2016].

4.4. Synthetic storm event generation

Once storm wave data were discretized by direction and linked to their respective climate forcing, synthetic storm event time series were generated for the two energy levels (moderate and high-energy) for the three directional groups (NE – E, E – SE, SE – S). Synthetic events were developed because there is considerable variability in the shape and duration of historical events. To relate sand transport patterns to storm energy and direction, idealised storm wave timeseries were required.

Within each energy/directional group, the storm closest to the observed median storm duration (92 h) was earmarked as the 'medoid storm' and used for designing a synthetic storm shape. The medoid storm was then idealised to derive a synthetic storm shape (Fig. 3). 'Hinge points' were marked delineating different sections (growth, peak, decay), and then a shape-preserving piecewise cubic interpolation was used between the hinge points. This was then smoothed using a Savitzy-Golay filter to return a more realistic storm shape. H_s values at each hourly interval were then normalised relative to the peak H_s so that a synthetic storm wave height time series could be built from any peak H_s value of choice.

Goda [2010] states that for locations where wind-waves are the major component of extreme waves, the storm wave period may be related to the storm wave height by:

$$T_s = \alpha(H_s)^{\beta} \quad (1)$$

where T_s and H_s are the significant wave period and height, and α and β are coefficients. Values of $\alpha = 6.5$ and $\beta = 0.33$ were suggested by Shand et al. [2011] to approximate T_p (rather than T_s) using H_s at the storm peak for storm wave events along the SEAS.

Examination of storm wave conditions in the buoy records suggest that within a single storm, T_p may increase with H_s, reaching a maximum

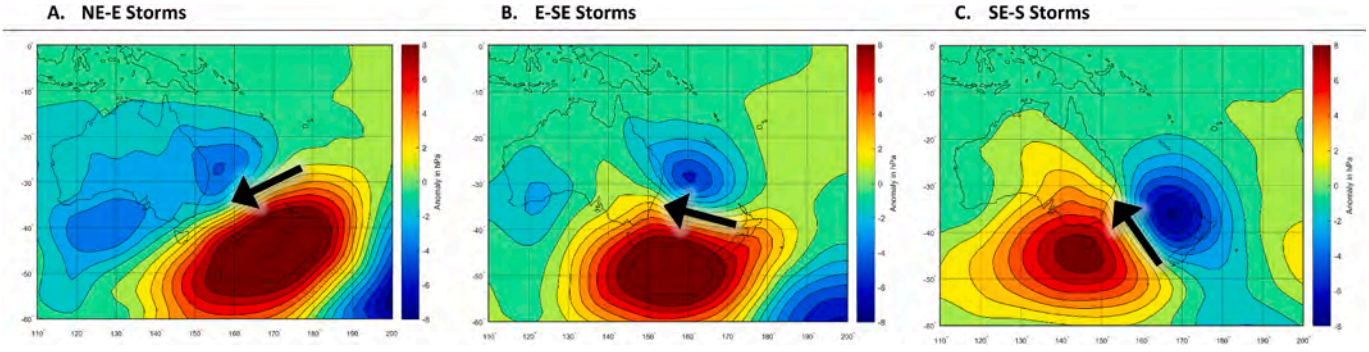

Fig. 2. Composite sea-level pressure anomalies over the Southwest Pacific for **a)** NE-E storm wave conditions, **b)** E-SE storm wave conditions, **c)** and SE-S storm wave conditions. Blue represents areas of anomalously low pressure (cyclonic in Southern Hemisphere) and red high pressure (anticyclonic). (For interpretation of the references to colour in this figure legend, the reader is referred to the web version of this article.)

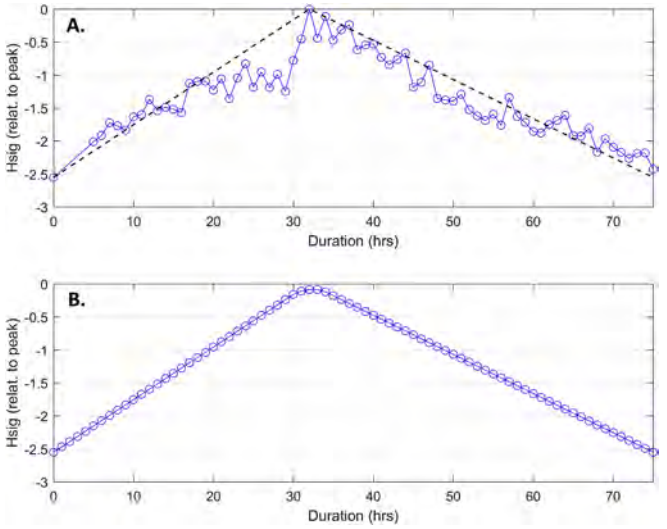

Fig. 3. Derivation of a synthetic storm shape from the medoid storm **a)** the medoid storm time series and idealised rising limb, peak and tail between hinge points; **b)** the smoothed synthetic timeseries at 1-h intervals. Note that hourly wave heights are expressed relative to the peak-storm wave height, meaning a synthetic storm event can be constructed from a single peak-storm value. This hourly resolution defines the model timestep.

around the time of the peak-storm H_s. Using this rule of thumb, the peak-storm T_p derived from Eq. (1), using the coefficients of Shand et al. [2011], was fitted to the synthetic storm shape in the same manner as the peak-storm H_s.

Using this method, synthetic storm wave time series were constructed from single peak-storm H_s and T_p values. Synthetic storms typical of moderate-energy storm conditions were constructed using the 50th percentile of peak-storm H_s and T_p values derived from the historical storm events collated within each of the three directional groups, and high-energy storms were constructed using the 95th percentile peak-storm H_s and T_p from the respective directional group.

The Annual Exceedance Probability (AEP) was also calculated for each synthetic storm event. The AEP of each 'moderate-energy' storm was based on the number of storms in the buoy record with peak-storm wave heights greater than the 50th percentile peak-storm wave height within the respective directional bin (NE-E, SE and S). The AEP of each 'high-energy' storm was based on the number of storms in the buoy record with peak-storm wave heights greater than the 95th percentile peak-storm wave height within the respective directional bin.

This process was repeated at both the wave buoy sites (Sydney and Byron Bay) to account for the differences in wave climate between the two locations. Table 3 details the peak-storm parameters used to generate each storm wave scenario, the resultant event durations, AEPs and accompanying peak-storm wind speeds.

The storm wave (and wind) directions were held constant through the duration of each synthetic event in the model and were defined as the median of all storm wave (wind) directions within each of the three directional sectors. In reality, the wave/wind direction will change through an event as the storm transits through the study area. However, the time-varying direction of storm waves were not included here as it inhibits the idealised analysis of climate forcing and sand transport.

Because the method for deriving synthetic storm wave time series is shape-preserving, storm events with higher (lower) peak-storm H_s have longer (shorter) durations – as occurs in reality. The storm durations derived here are broadly comparable with those developed by other authors [Carley and Cox, 2003; Shand et al., 2011]. For example, for peak-storm H_s of 5.7 m and 7.5 m, these authors derived a synthetic duration of ~90 and ~ 120 h, respectively. In this study, durations for comparable peak wave heights are ~110 h and ~ 170 h. While our storms are longer, they are still well within the observed range for events of these magnitudes (up to ~200 h). This is because we use a shallower storm tail (derived from observations), while previous authors have derived the storm shape from exceedance heights of different durations, which results in a steeper tail.

4.5. Wind forcing

Strong winds often accompany extreme wave events, and wind-driven currents contribute to sand transport in addition to waves along the SEAS [Griffin et al., 2008]. Local winds also transfer high-frequency energy to wave spectra which in turn influences wave-driven sand transport.

A regression of storm wave heights recorded at the wave buoys against the upscaled CFSR winds extracted at the buoy locations showed that higher storm wave heights are generally accompanied by higher wind speeds. A cross-correlation analysis showed that in general, wind speeds varied within the same hourly time step as wave heights during a storm.

In light of this, peak-storm wind speeds were scaled in relation to the peak-storm wave heights using a linear regression function, and then distributed on the same curve as used for the storm wave height time series, to simulate the growth and decay of winds through the storm. Wind direction, like wave direction, was held constant through the storm.

5. Modelling approach

5.1. Description of models used

The MIKE 21 suite of models developed by the Danish Hydraulic Institute (DHI) was used. A wave model (MIKE 21 Spectral Wave SW) was dynamically coupled to a flow model (MIKE 21 Flow Model HD) and a sediment transport model (MIKE 21 ST), to simulate wind and wave-driven currents, sediment transport and morphological change. An 'online' dynamical coupling between waves, currents and morphology was performed at each grid cell and time step.

MIKE 21 SW simulates the growth, decay and transformation of

Table 3
Peak-storm parameters used to generate each storm wave scenario, the resultant event durations and accompanying peak-storm wind speeds. Wave heights (H_s) are in m, wave periods (T_p) in s, wind speeds (u) in ms^{-1}, storm durations (*dur.*) in h., and wave/wind directions in ° TN. *AEP* refers to Annual Exceedance Probability.

Directional sector	Moderate-energy storms (50th percentile of all storms)					High-energy storms (95th percentile of all storms)					Wave and wind direction
	H_s (m)	T_p (s)	u (m/s)	dur. (hrs.)	AEP	H_s (m)	T_p (s)	u (m/s)	dur. (hrs.)	AEP	
— Sydney (Central Coast NSW) —											
NE – E	4.1	10.4	10.1	63	0.19	5.6	11.5	12.4	107	0.02	86
E – SE	3.9	10.2	9.9	56	0.50	6.0	11.7	13.0	118	0.05	128
SE - S	4.0	10.3	10.0	60	1.80	6.1	11.8	13.2	121	0.18	169
— Byron Bay (Far-North Coast NSW) —											
NE – E	4.0	10.3	10.0	59	0.25	7.6	12.7	15.4	166	0.02	93
E – SE	4.2	10.4	10.3	63	0.65	6.5	12.1	13.8	133	0.07	128
SE - S	3.8	10.1	9.7	54	1.60	5.1	11.1	11.7	92	0.16	165

wind-generated waves and swell in offshore and coastal areas [Danish Hydraulic Institute [DHI, 2022a]. The directionally-decoupled and quasi-stationary solutions were used. These were found to be the more stable solutions and are recommended for instances of fetch-limited wave growth [Danish Hydraulic Institute [DHI, 2022b]. As a result, white-capping, triads and quadruplet harmonics were excluded; results are therefore unsuitable for very shallow (depth, $d <$ wavelength, $L/20$) and very deep water ($d > L/2$) where these processes may dominate. A phase-decoupled refraction-diffraction approximation [Holthuijsen et al., 2003] was also used.

MIKE 21 HD is a 2D non-hydrostatic model based on the depth-integrated, Reynolds-averaged Navier-Stokes equations [Danish Hydraulic Institute [DHI, 2022b]. A 2D implementation is usually sufficient for coastal applications where the water column is fully mixed, away from river estuaries and other outlets, where the assumptions of Boussinesq and hydrostatic pressure can be invoked. The 2D implementation assumes, therefore, that bottom flows (like the East Australian Current, EAC) do not contribute to shoreface sand transport.

Sediment transport due to combined currents and waves was calculated using MIKE 21 ST. Transport rates are found a priori from linear interpolation in a multi-dimensional transport table, generated by a quasi-3D model (STPQ3D). Bed load is calculated according to the model of Engelund and Fredsøe [1976]. Suspended load is based on the diffusion equations of Fredsøe et al. [1985]. Transport calculations are 'quasi-3D' because they are derived from the mean horizontal velocity component, which is equal to the depth-averaged velocity from 2D hydrodynamic simulations. Modelled sediment transport rates in this study are uncalibrated to observations.

Details regarding model calibration against pre- and post-storm observations for an East Coast Low event in 2016 at Narrabeen, are provided in Supplementary Information.

5.2. Model extents and resolutions

Two regional models (central coast NSW, and north coast NSW) were set up to capture the regional wind and wave climate, and shelf characteristics likely to influence transport processes at the three study sites. Both models were based on a series of irregular (flexible mesh, FM) elements which allowed a variable resolution within the domains.

The models extended in a cross-shore direction from the landward edge of the subaerial beach to the 60-m isobath. This depth contour is widely regarded as the boundary between the lower shoreface and inner shelf along the SEAS [Roy and Stephens, 1980]. There is no evidence to suggest that sand is exchanged across this boundary, and sediment sampling [Ribó et al., 2020] suggests that sediment grades to cohesive muds beyond this point.

The central coast model extended approximately 50 km alongshore from North Head, at the entrance to Sydney Harbour, to Forresters Beach, on the central NSW coast (Fig. 4). The regional mesh graded from an approximate 200 m element length at the offshore boundary, to 50 m at the land boundary. Two higher-resolution areas covering the Narrabeen and Wamberal embayments were nested within the regional mesh. These areas extended to the 40 m isobath at both sites, and had a maximum element length of 20 m.

The north coast domain extended approximately 35 km alongshore from Lennox Head, south of Byron Bay, to just north of the Brunswick River (Fig. 5). The regional mesh was set up in a similar fashion to the central coast domain. A nested high-resolution area was centered on Cape Byron, extending north to Belongil Beach, extending to the 40 m isobath with a maximum resolution of approximately 20 m.

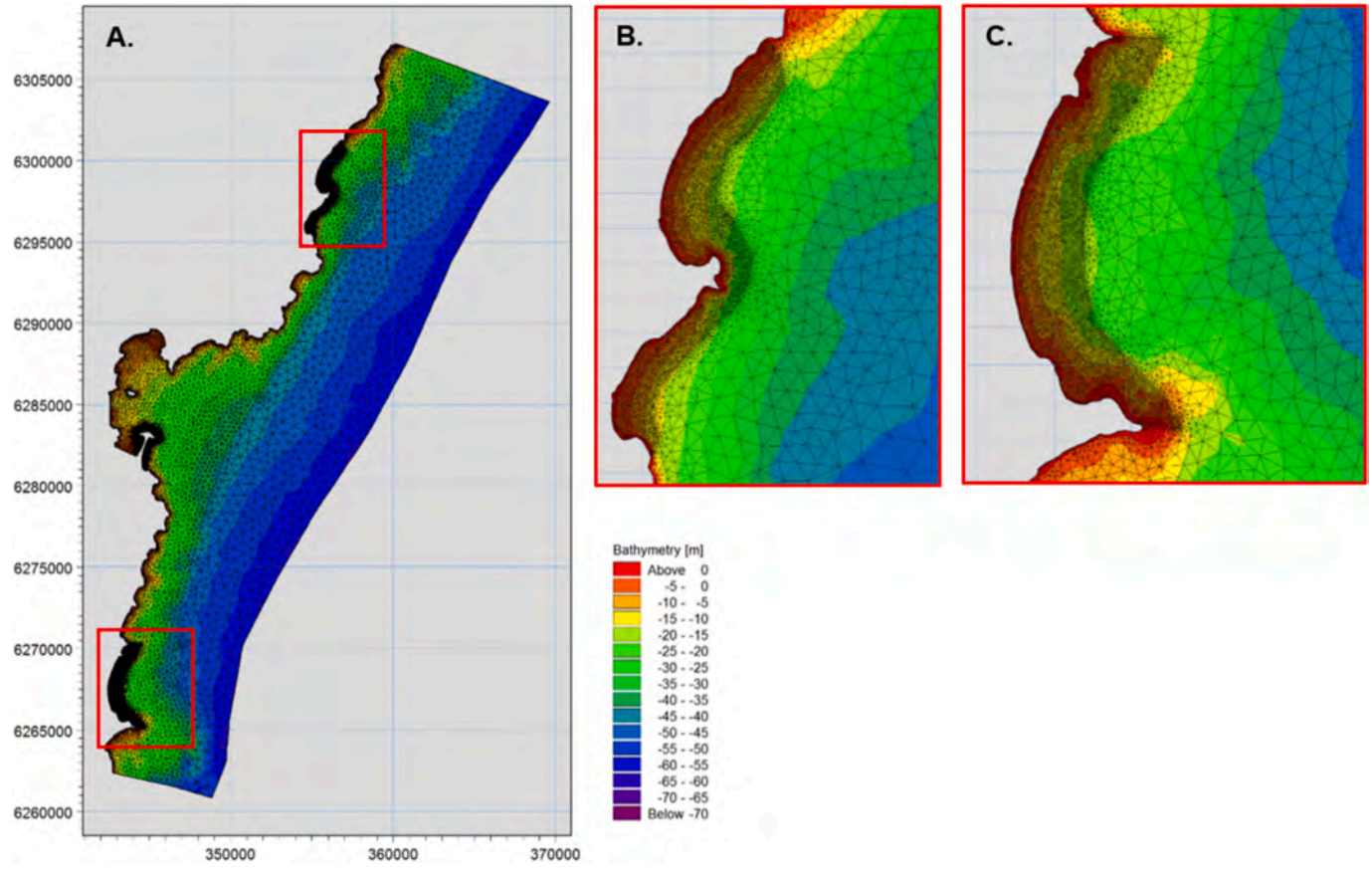

Fig. 4. Central Coast NSW model (A) showing high resolution mesh areas for Wamberal (B, and northern red box in A) and Narrabeen (C, and southern red box in A). (For interpretation of the references to colour in this figure legend, the reader is referred to the web version of this article.)

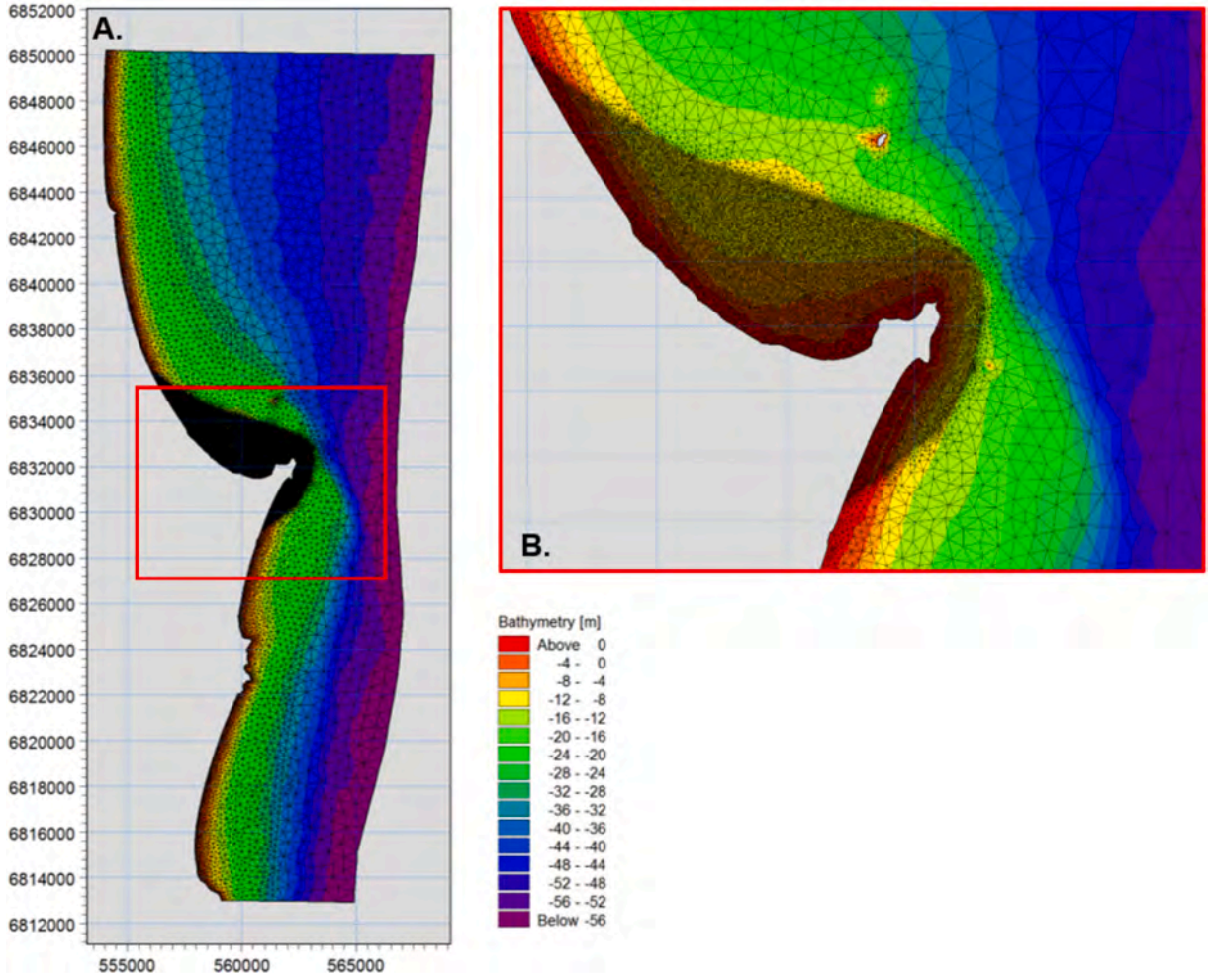

Fig. 5. North Coast NSW model (A) showing high resolution mesh areas for the Byron Bay area (B, and red box in A). (For interpretation of the references to colour in this figure legend, the reader is referred to the web version of this article.)

5.3. Seabed parameterization

Variable bed characteristics were used in modelling to account for different seabed types on the shoreface. Areas of sand and reef were digitized from Ribó et al. [2020] and parameterized in terms of flow resistance, bottom friction, available erodible material and potential for transport.

Given the uncertainties in cross- and alongshore sand characteristics, a single grain size distribution and bottom roughness were used for areas of sand in each model domain. The grain size distribution was described by the median grain diameter, d_{50}, and a grading coefficient, α. A d_{50} of 0.33 mm (0.22 mm) and α of 1.34 was used for areas of sand in the central (north) coast model, representing mean regional values from an analysis of ~800 sediment samples along the NSW shelf in Ribó et al. [2020]. A hydraulic roughness (k_n) of 0.04 m was used to represent the existence of small sand ripples [Weber, 1991], which equates to a Manning's M (the reciprocal of Manning's n) of 45 for bottom friction. The erodible bed layer thickness over areas of sand was set at 10 m, which is essentially an infinite thickness over the duration of a single storm event.

For areas of rock reef, bed roughness was estimated from lidar-derived transects of exposed rock platforms around Long Reef and Terrigal headlands. The consecutive substratum height difference was calculated along reef flat transects after McCormick [1994] and the standard deviation used to estimate the physical roughness height, k_w after Lowe et al. [2005]. k_w ranged from 0.08 to 0.33 m, with the median of 0.16 m used. These are slightly larger than those reported for coral reefs – for example, 0.06–0.07 m by Nelson [1996] and 0.14–0.16 m by Lowe et al. [2005] - reflecting the greater rugosity and variability of bare rock reefs. k_w was then used to estimate k_n (the hydraulic roughness), assuming that for reef $k_w \approx d_{50}$ after Lowe et al. [2005], and so $k_n \approx 2\,k_w$ after Nielsen [1992]. Thus, a k_n of 0.32 m was used for reef areas, equating to a Manning's M of 32. The erodible bed layer thickness over reef was set to zero.

6. Validation against observed long term bed elevation change

6.1. Morphological upscaling

Bed elevation change on the sub-aerial beach and surf-zone may vary on the order of tens of centimetres to metres over a single storm event [e.g. Bracs et al., 2016]. The transfer of sand from the lower shoreface to the upper shoreface and shoreline, however, occurs at a much smaller rate over much longer timescales, equivalent to a sand grain thickness [Kinsela et al., 2016]. While this is negligible for beach systems on the event-scale, it may constitute an important transport pathway when integrated over decades to millennia.

A key challenge of modelling sand transport on the lower shoreface is the efficient application of process-based models to investigate small-scale change over long time periods. It is not possible to run a continuous morphological model over centennial time scales because of processing time. Even if it were possible, it would largely be a waste of time

because sand transport in deep water is episodic, only occurring during infrequent and high-energy events [Harris and Wiberg, *2002*].

As highlighted, morphological upscaling has been used before in a variety of forms to model long term coastal processes [e.g., Cowell et al., 1995; Roelvink, 2006; Ranasinghe et al., 2011]. However, in no previous work has morphological upscaling been linked to regional atmospheric drivers and resultant directional wave climate. Here, event scale samples of the wave and wind climate are discretised by magnitude and direction (described in Section 4), run through a morphological model, and upscaled to the timescale of interest using a weighted morphological scale factor:

$$\Delta d = nAEP(\Delta d_s) \quad (2)$$

Where Δd is the cumulative long-term bed elevation (depth) change, n is the total number of years to be modelled, *AEP* is the annual exceedance probability of the storm type and Δd_s is the modelled bed elevation (depth) change after a single storm event. *AEP* is estimated from wave buoy observations as per Table 3.

There are two limitations of this approach. First, scaled bed elevation change is only applicable for areas seaward of the surf zone. This is because over long timescales, non-storm (modal) wave conditions that occur between storms, re-work sediments over the subaerial beach and surf zone. Upscaling morphological change from a single storm event within the surf zone leads to unrealistically large volumetric change because the interceding modal conditions are not accounted for. For depths outside the surf zone, where modal wave and wind conditions do not have sufficient energy to move sand, the a priori assumption is that the upscaled storm-induced bed elevation changes are likely to be more akin to the real net observed change. The assumption is that all change in shallow water reduces to a long-term equilibrium in line with the modal (non-storm) wave climate, while morphological change outside the surf zone is the integral of storm wave events over the long term [Niedoroda et al., 1984; Pemberton et al., *2012*; Anthony and Aagaard, *2020*]. Second, the modelled upscaled change on the lower shoreface does not account for updated bathymetry after each successive storm event. This means that the "chronology effect" of storm wave events that in reality impact the net observed change, were not accounted for.

6.2. *Spatial patterns of storm-driven morphological change on the lower shoreface at Byron Bay*

Goodwin et al. [2013] compared bed elevation change around Cape Byron using a hydrographic survey conducted in 1883 that used lead-line soundings, with a bathymetric LiDAR-derived survey undertaken in 2011 (128 years difference). The total vertical uncertainty attributed to the digital surface of the difference between the two surveys was approximately +/− 0.5 m. Over this period, the hindcast wave climate was from the south-east quadrant but with significant interdecadal variability [Goodwin et al., 2013]. Subsequent reconstruction of sea-level pressure anomalies over this period also shows that there was a higher frequency of SE storm events than at present [Browning and Goodwin, *2013*].

We assume that lower shoreface change observed over this ~130-year period is the integral of high-energy storm wave events. First, we compared the pattern of observed morphological change to the modelled storm scenarios from the three directional quadrants (N*E*-N, E-SE and SE-S). The spatial pattern of change is primarily controlled by the wave direction. The areas of net accumulation (red) and erosion (blue) were extracted from the modelled results and the polygons were smoothed for ease of comparison (Fig. 6). The same was done using the original observations used by Goodwin et al. [2013].

An important point of calibration is determining an appropriate lower bound threshold of morphological change to regard in the model as 'error' and to not include in the comparisons. To do so, we truncated the distribution of morphological change across the domain for each model run to the inter-quartile range (IQR). Almost all small-scale bed elevation change within the IQR occurred on the lower shoreface. In each case, the truncated distribution was skewed towards negative values – indicative of small-scale bed lowering on the lower shoreface and landward transport. This conforms with Navier-Stokes theory of wave asymmetry in deep water leading to skewed wave-induced orbital motion and shoreward transport.

After some testing, it appeared that one standard deviation around zero using the truncated (IQR) model distribution, returned the best results when compared to the spatial pattern of observed seabed change.

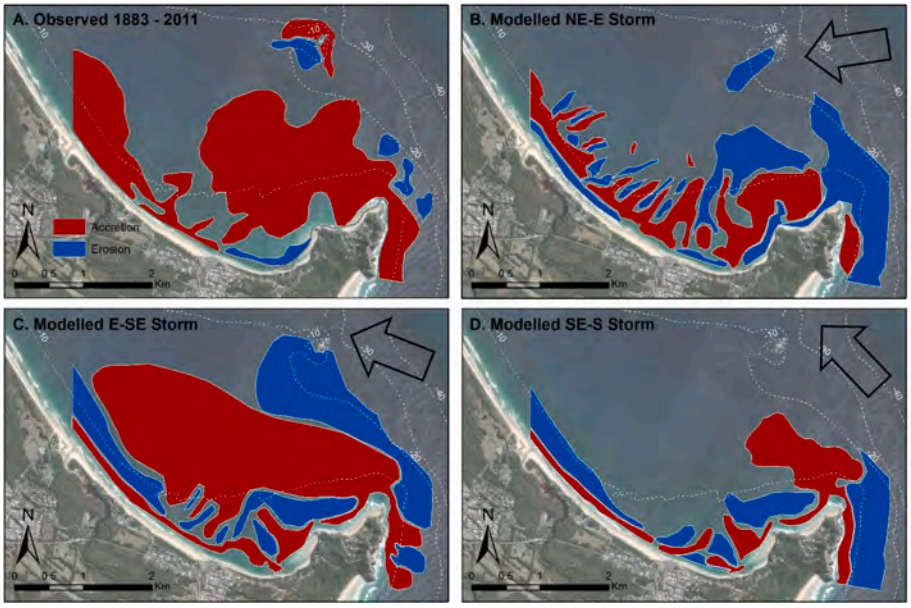

Fig. 6. Comparison of observed (A) and modelled (B, C, D) patterns of long-term seabed change on the lower shoreface around Cape Byron and into Byron Bay. Storm events are modelled from the NE-E (B), the E-SE (C) and the SE-S (D). Areas of red indicate net positive seabed change (accumulation) and areas of blue indicate net negative seabed change (erosion). Only areas of 'significant' change are shown (see text for explanation). Modelled storm wave direction is denoted by arrows in top right of panels (B) to (D). The present day 10, 20, 30 and 40-m isobaths are also shown in each plot for comparison. The same area of the lower shoreface is compared in each case. (For interpretation of the references to colour in this figure legend, the reader is referred to the web version of this article.)

This equated to +/− 0.005 to 0.03 m for different storm scenarios depending on the magnitude of sand transport that occurred in each. This range was omitted for each storm scenario, leaving what we regard as 'significant' patterns of change in Fig. 6.

Fig. 6 indicates that the SE storm scenario returns the best match with the pattern of observed bed level change, unsurprising given that the period 1883–2011 was dominated by south-easterly wave conditions [Goodwin et al., 2013; Browning and Goodwin, *2013*]. The model captures the general extents of the shore-parallel accretion observed off Cape Byron between 5 and 15 m depth, and the orientation and approximate depth limits of the lower shoreface accretion lobe (bypass strand) north of Cape Byron. The model appears to over-estimate the northward extent of the bypass strand and does not capture the lobe of accretion observed extending to approximately 15 m water depth to the far north-west of the observed difference model. This is because this feature represents the growth of the ebb-tidal delta from Belongil Creek, which is not included in the model. Outflow from the creek and the resulting nearshore current field may have stunted the northward growth of the bypass strand, hence the difference between observed and modelled results to the northwest of the model domain.

6.3. *Volumetric change and sediment transport pathways on the lower shoreface at Byron Bay*

Next, we look to evaluate whether the upscaled modelled results can reasonably replicate the centennial-scale volumetric change observed outside the surf zone at Byron Bay. Here we are not looking for exact replication because this is a parameterised solution that will ultimately not capture all the boundary forcing over the period 1883–2011. For example, we do not include the sequencing of storm wave events or morphological evolution over the 128-year period, nor running the model on the 1883 bathymetry. In addition, while we have replicated the method of volumetric calculation used in Goodwin et al. [2013], there is uncertainty associated with comparing volumetric results due to the much denser data point cloud produced with modelling, requiring less interpolation, than for the surveyed results.

The aim of this comparison is to test the theory that the morphological signal can be modelled by parameterising the principal agent (storm waves) and upscaling it. It also supports our understanding of sediment transport pathways and directional storm wave events at this site.

Goodwin et al. [2013] divided the Byron Bay shoreface into ten morphological areas shown in Fig. 7. Here we test the model for those areas that are wholly outside of the surf zone and therefore more likely to reflect high-energy storm wave driven seabed change (red shaded areas in Fig. 7). We compare the surveyed 1883–2011 volumetric change in each of these four areas with the upscaled model results under all six storm scenarios. Results are given in Table 4.

Table 4 shows that the upscaled modelled results can produce volumetric change that is of a similar order of magnitude as the observations, depending on the directionality and magnitude of the storm wave conditions. This provide some confidence in the morphological scale factors, noting that the AEP estimate for each storm event is derived from the available observational wave data period at Byron Bay and assumes that this probability is reflective of the longer-term (i.e., centennial-scale) wave climate.

For the "Outer Nearshore 1" zone, similar levels of net accretion as those observed can only be replicated under the high-energy E – SE storm conditions and is still smaller than observed even after upscaling. We note that the model is not using the 1883 bathymetry which may

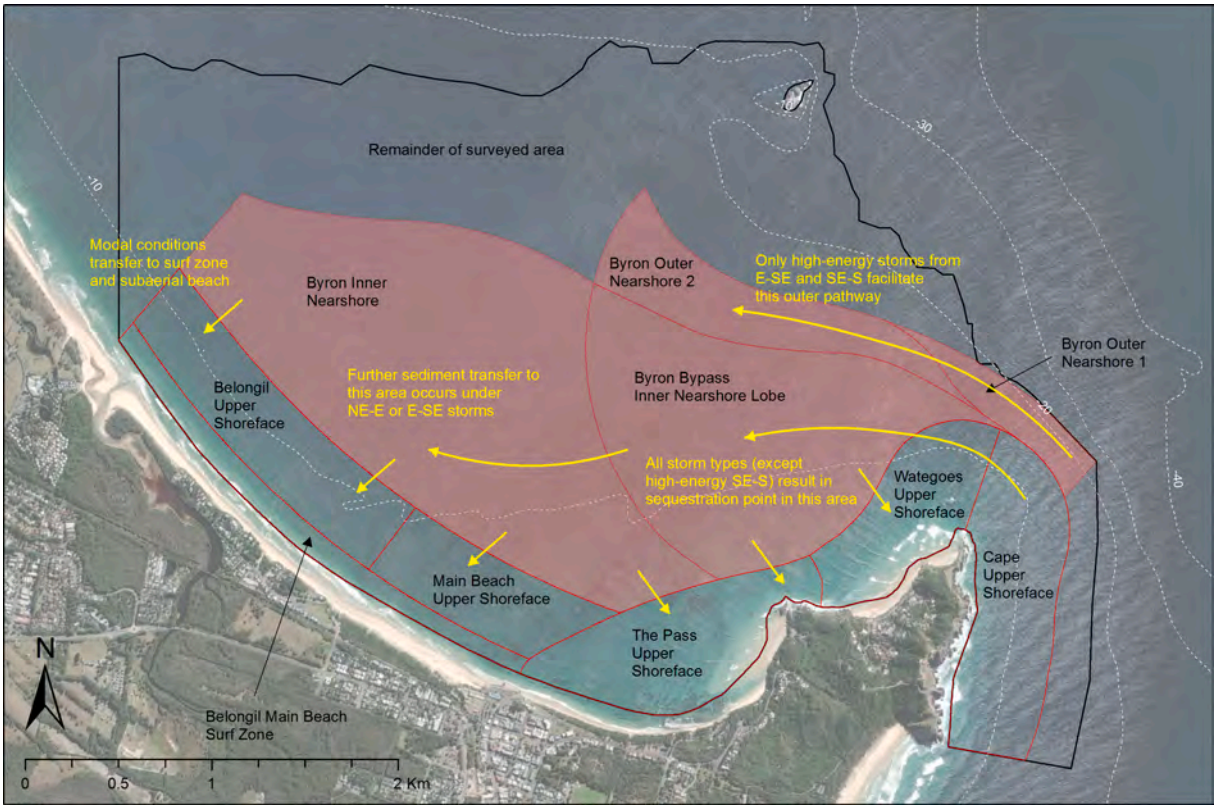

Fig. 7. Morphological areas and storm wave transport pathways across the shoreface at Byron Bay. Surveyed bed elevation change over the period 1883–2011 was compared to upscaled model results for all areas that are wholly outside of the surf zone (red filled areas in above image). Black line shows the total common surveyed area. Sediment transport pathways and storm wave drivers, deduced from model results, are shown in yellow arrows and text. The present day 10, 20, 30 and 40-m isobaths are also shown. Morphological areas are taken from Goodwin et al. [2013]. (For interpretation of the references to colour in this figure legend, the reader is referred to the web version of this article.)

Table 4
Observed and modelled volumetric change at Byron Bay over the period 1883–2011. Volumes are in 10^3 m^3, rounded to the nearest 1000 m^3. 'High' refers to high-energy storms and 'Mod.' refers to moderate-energy storms.

Morphological Area	Surveyed change 1883–2011 (10^3 m^3)	Upscaled modelled storm results (10^3 m^3)					
		NE-E		E-SE		SE-S	
		Mod.	High	Mod.	High	Mod.	High
Byron Outer Nearshore 1	43	–	–	–	10	–	–
Byron Outer Nearshore 2	118	–	–	–	–	128	–
Byron Bypass Inner Nearshore Lobe	1106	–	–	1164	1965	–	–
Byron Inner Nearshore	597	32	59				

have had an additional sediment supply around the Cape thus increasing the potential for higher accretion in this area. Wave-current interactions are also important to sand deposition around Cape Byron. It has been previously identified that the southward flowing Pacific western boundary current, known as the East Australian Current, impinges on the middle to inner shelf and interacts with the longshore transport in this location [Ferland, 1990; Roy, 1998; Bickers, *2004*]. This wave-current interaction is not in our modelling, neither is the effect of bottom currents, as these are averaged out across the water column in our two-dimensional model.

For the "Outer Nearshore 2" zone, the model best replicates the observed net accretion under the moderate-energy SE – S storm scenario. This suggests that the net accretion observed in this area is only possible in oblique storm wave conditions and may be the result of winnowing from the Outer Nearshore 1 area under sequential SE – S storm wave events.

For the "Byron Bypass Inner Nearshore Lobe" zone, net accretion (as observed) can occur under E – SE storm scenarios. This suggests long term bed elevation change in this area is the result of predominantly storm wave events from the E – SE quadrant.

For the "Byron Inner Nearshore" zone, net accretion (as observed) only occurs under the NE – E storm scenarios. However, these storm events alone only account for a very small portion of the total observed net accretion in this area over the centennial period. There is likely significant movement of sand during non-storm (modal) wave conditions in this shallow water area, which is not accounted for in our storm-focused model.

Model results using morphological upscaling are consistent with there being two major sediment transport pathways into Byron Bay (as shown in Fig. 7). The first is from the Outer Nearshore 1 area to Outer Nearshore 2, facilitated by E - SE storm wave transport. The second is around Cape Byron to the Nearshore Lobe, which appears to be a sequestration point under almost all storm wave directions and magnitudes. Some of this volume can be subsequently transferred to Quthe

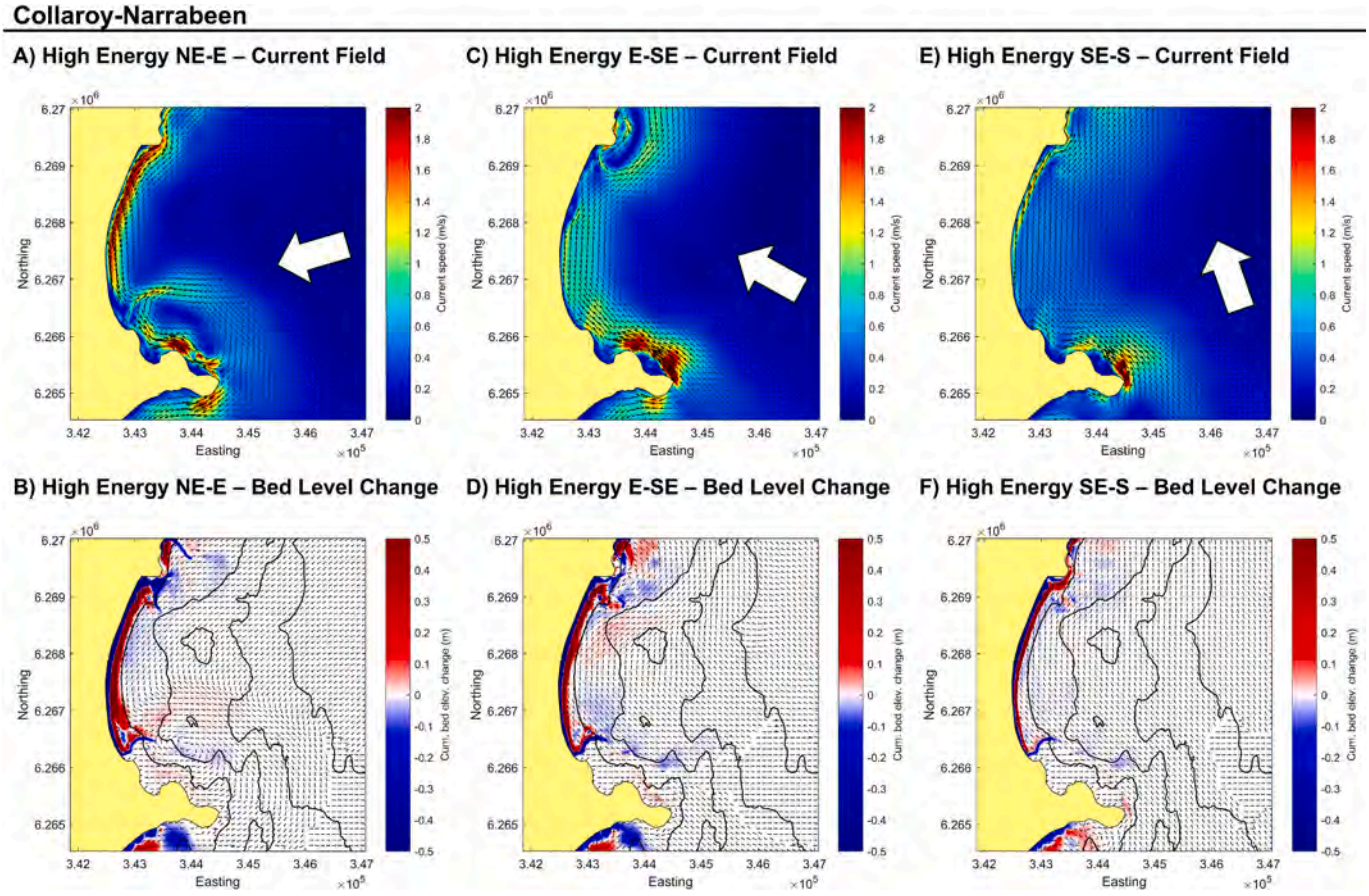

Fig. 8. Peak storm current field (A, C, E) and cumulative bed elevation change after centennial morphological upscaling (B, D, F) for high energy NE-E (A, B), E-SE (C, D) and SE-S (E, F) wave and wind scenarios for Collaroy-Narrabeen. Wave vectors on (A, C, E) denote peak-storm wave direction for each scenario. Isobaths on (B, D, F) show 10, 20, 30 and 40 m depths.

Inner Nearshore area during NE – E storms. From here, modal wave conditions can rework this sediment into the surf zone and subaerial beach.

7. Results and discussion

The synoptic typing/morphological upscaling approach as described above, was then applied to other coastal compartments along the SEAS. Given the scarcity of observations of centennial-scale bathymetric change, model performance at the below sites cannot be directly validated as at Byron Bay. It is therefore an assumption of this work that model performance at Byron Bay is comparable to other sites. As a result, we only discuss the large-scale modelled patterns at these sites below. Quantitative metrics for each of the below study sites are provided in Supplementary Information.

Figs. 8 and 9 show the modelled current field (at the peak of the synthetic storm) and resultant cumulative bed elevation change after centennial-scale morphological upscaling, for the three high-energy directional storm wave regimes (N*E*-E, E-SE, SE-S), for Narrabeen and Wamberal. Modelled results for "moderate" storm wave conditions, and other sites along the SEAS, are provided in Supplementary Materials.

7.1. Collaroy-Narrabeen

During periods of N*E*-E storm wave conditions, generated by a NE/SW oriented blocking high pressure system in the Tasman Sea with a tropical low-pressure trough to the north (Fig. 2), a large-scale rip circulation is produced in the southern third of the Narrabeen embayment, fed by alongshore currents feeding in from both the north and south. The current bifurcates at Long Reef headland to the south of the embayment. Modelling suggests these high energy episodic transport conditions - occurring on average only twice over a 100-year period under current wave climate conditions (Table 2) - can lead to significant offshore transport and deposition of sediment from the upper shoreface and subaerial beach out to depths of 30 m in the southern third of the embayment.

Under present-day sea-level conditions, it is unclear how sediment deposited at this location could be reworked back onto the shoreline. Modelling results from *E*-SE and SE-S storms indicate no significant bed elevation change occurs at this location between the 20 and 30-m isobaths. It is possible that storms of higher magnitude than those modelled could winnow sediment from this location, but given their rarity, this would not lead to significant change over the centennial scale. We may conclude, therefore, that this would remain as a relict deposit of "disequilibrium stress" that could only be moved shoreward during periods of lower sea level than today.

Results also indicate that a long-term embayment rotation signal may occur on the lower shoreface under differential N*E*-E and E-SE storm wave conditions. Numerous studies have shown that embayment rotation can occur across the subaerial beach and upper shoreface under directional wave climate forcing on the event to seasonal scale [e.g. Harley et al., *2015*; Bracs et al., *2016*]. This study indicates that a longer-term, smaller scale signal of the same sign may also be detectable across the lower shoreface on centennial timescales, driven by episodic, extreme storm wave conditions. During NE-E storms, an anti-clockwise rotation of the lower shoreface occurs, with positive bed elevation change occurring to the south and negative change to the north. During E-SE storms, the inverse pattern occurs, leading to a clockwise rotation of the lower shoreface.

High energy storm wave conditions from the SE-S quadrant are too oblique to have any significant impact on bed elevation change across the lower shoreface at Narrabeen. Storms from these directions may be

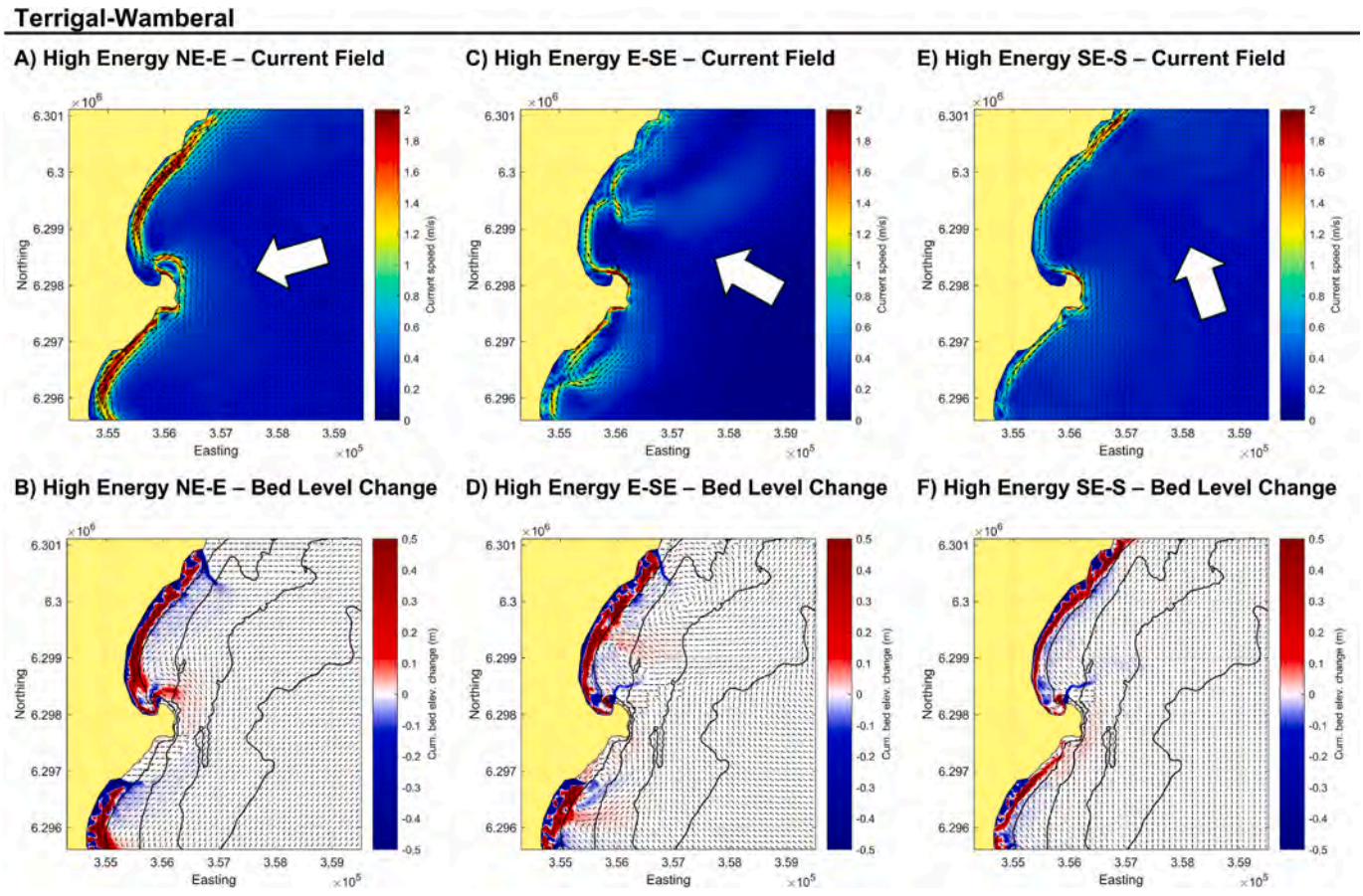

Fig. 9. As Fig. 8, for Terrigal-Wamberal, also showing Avoca compartment to the south of Terrigal headland.

agents of alongshore transport within headland-contained compartments, but do not appear to influence the long-term pattern of lower shoreface change which is predominantly a cross-shore signal.

7.2. Terrigal-Wamberal

At Wamberal, under the same atmospheric and N*E*-E wave climate forcing as at Narrabeen, a rip circulation cell is also produced but the offshore current does not fully recirculate and instead feeds into the southward flowing alongshore current that is pushed across Terrigal headland and into the Avoca compartment to the south. The location of the rip cell is also further in the lee of the N*E*-Esouthern hook of the embayment, than at Narrabeen, due to the more oblique orientation of the embayment with respect to the wave direction. This flow pattern promotes the deposition of a headland-attached lobe of sediment north of Terrigal headland, which grades down to the 30-m isobath. A centennial scale, anti-clockwise rotation of the lower shoreface is also detectable, as seen at Narrabeen.

E-SE conditions are shore-normal at Wamberal and set up a recirculatory current in the middle of the embayment which leads to a pattern of positive bed elevation change in the central corridor of the lower shoreface. These hydrodynamic conditions strip sediment across the shoreface in both the north and south sections of the embayment from around 10–15 m depths, jettisoning it in a shore-normal direction in the middle of the embayment out to around 30 m depth.

As is the case at Narrabeen, modelling suggests that SE-S storm wave conditions are too oblique to force a significant centennial scale response on the lower shoreface at Wamberal. However, under both SE-S and E-SE storm conditions, a pattern of erosion is seen emanating in a north-eastward direction from Terrigal headland out to the 20-m isobath. This may represent the diffraction and wave breaking processes that occur in the lee of the headland during southerly oblique storm wave conditions, and the bed lowering that ensues along the outer edge of the subaqueous portion of the reef as waves break and propagate shoreward. The “blue finger” visible in Fig. 9 D and F to the north of Terrigal headland illustrates how far out in the embayment this process can extend to, in terms of producing significant bed elevation change when accumulated over the centennial-scale.

It should be noted that for all atmospheric-storm wave scenarios, at both Narrabeen and Wamberal, a cross-shore pattern of negative bed elevation change (deep blue) at the toe of the subaerial beach, and positive bed elevation change (deep red) at depths <10 m, takes place. This represents the process of scour and bar building which is the typical net sign of change on the upper shoreface during storms of all directions at the event scale.

However, for the purposes of this discussion, and as described in Section 6, we disregard all modelled change on the upper shoreface because sediment at these depths will be redistributed outside of storm events by modal wave conditions. By comparison, the morphological “signature” of storms on the lower shoreface remains intact until the next storm, because modal wave conditions do not have sufficient energy to transport sediment at these depths. It is these lower shoreface morphological signatures – and their linkage back to synoptic climate forcing – that is the focus of this paper.

8. Conclusions

This study presents a novel approach to determine the long-term, lower shoreface morphological response to regional climate forcing, using a combination of synoptic wave climate typing, coupled wave-hydrodynamic-sediment transport modelling, and frequency-based morphological upscaling, to produce a causal network for risk-based scenarios.

We find that at all sites and under the most extreme storm wave conditions modelled, the 30–35 m depth zone appears to be the ultimate seaward limit of significant, shoreward sediment transport on the centennial scale. This is beyond the depth of closure (DoC) on the upper shoreface of around 14 m at Narrabeen [Harley et al., *2022*] and 12 m at Wamberal [Couriel, *2021*]. It is, however, consistent with other observational based studies [e.g., Hallermeier, *1981*; Valiente et al., *2019*] that have investigated the maximal limit of shoreface sediment transport under extreme wave forcing.

The DoC is typically considered the lower design limit for closing the sediment budget for coastal engineering applications [U.S. Army Corps of Engineers, 2012], and there is typically no consideration of sediment movement beyond this depth. This study suggests that, for coastal infrastructure projects on the Southeast Australia Coast (with typical design lives of over 50 years), some significant sand transport impacting the coastal sediment budget occurs beyond the DoC, out to the ~30-m depth. For these studies, we recommend that the sediment transport processes should be considered out to ~30-m depth to fully account for design life relevant conditions.

This also indicates that, under present-day sea-level conditions, inner shelf sediment deposits located beyond the toe of the lower shoreface (30 to 35 m isobaths) are relict and inactive with regards to the centennial scale sediment budget of coastal compartments along the Southeast Australian coast. This is an important consideration for coastal managers when considering offshore locations for sand extraction for beach nourishment projects and ensuring that any extraction does not adversely impact the coastal sediment budget.

This study also demonstrates that only storms with quasi-coast normal directions are able to force significant sediment transport on the lower shoreface. In the case of the Southeast Australian Coast, storms clockwise of SE, while potentially important mechanisms for headland bypassing and alongshore transport on the upper shoreface [e.g. Silva et al., *2025*], are too oblique to be agents of long-term, cross-shore episodic sediment transport from the lower shoreface to the coast.

The approach presented in this paper provides practitioners with a causal network approach that offers a linkage between the major modes of regional atmospheric and wave climate variability, and their long-term morphological response across the shoreface. By focusing on the extreme, episodic wave events as the principle agent for cross-shoreface sand transport, it can be used to link either future climate model projections of synoptic weather patterns over the coming century, or paleoclimate reconstructions of past centennial periods, to sand transport pathways across the shoreface.

CRediT authorship contribution statement

T.R. Mortlock: Writing – review & editing, Writing – original draft, Validation, Software, Methodology, Investigation, Data curation, Conceptualization. **I.D. Goodwin:** Writing – review & editing, Supervision, Project administration, Methodology, Investigation, Funding acquisition, Conceptualization. **M. Ribó:** Writing – review & editing, Formal analysis, Data curation, Conceptualization.

Declaration of competing interest

The authors declare the following financial interests/personal relationships which may be considered as potential competing interests: Thomas Mortlock reports financial support was provided by New South Wales Environment and Heritage. If there are other authors, they declare that they have no known competing financial interests or personal relationships that could have appeared to influence the work reported in this paper.

Acknowledgments

This research was funded by a NSW Office of Environment and Heritage (OEH) grant to CI Goodwin as part of the OEH/Sydney Institute of Marine Science (SIMS), Coastal Processes and Response Research Node (Grant Project 1 A Quantification of Sand Supply from the NSW

Shoreface). We would like to thank colleagues at OEH for their direction at various stages of the work, and technical support from DHI Water & Environment.

Appendix A. Supplementary data

Supplementary data to this article can be found online at https://doi.org/10.1016/j.margeo.2026.107733.

Data availability

Wave data from Waverider buoys in New South Wales (NSW) and tidal data from the HMAS Penguin tide gauge are collected as part of the NSW Coastal Data Network Program managed by OEH and were sourced from Manly Hydraulic Laboratory. Hindcast wind data was obtained from the NCEP Climate Forecast System Reanalysis (CSFR) portal at https://rda.ucar.edu/datasets/. The NOAA Twentieth Century Reanalysis (20CR) product was also used, from https://www.esrl.noaa.gov/psd/data/20thC_Rean/. All bathymetric data used for modelling was provided by OEH for this study. A Macquarie University academic licence for MIKE by DHI software was used for modelling. All synthetic storm wave and wind scenarios, wave modelling data and outputs presented in this work can be obtained from t.mortlock@unsw.edu.au.

References

Anthony, E.J. and T. Aagaard (2020), The lower shoreface: morphodynamics and sediment connectivity with the upper shoreface and beach. Earth Sci. Rev., 210 (103334), doi:https://doi.org/10.1016/j.earscirev.2020.103334.

Bickers, A., 2004. Cape Byron habitat mapping, Cooperative Research Centre for Coastal Zone, Estuary and Waterway Management Report, Indooroopilly Queensland, Australia, p. 37.

Bracs, M.A., Turner, I.L., Splinter, K.D., Short, A.D., Mortlock, T.R., 2016. Synchronised patterns of erosion and deposition observed at two beaches. Mar. Geol. 380, 196–204. https://doi.org/10.1016/j.margeo.2016.04.016.

Browning, S.A., Goodwin, I.D., 2013. Large-scale influences on the evolution of winter subtropical maritime cyclones affecting Australia's East Coast. Mon. Weather Rev. 141 (7), 2416–2431. https://doi.org/10.1175/MWR-D-12-00312.1.

Cardno, 2012. NSW Coastal Waves: Numerical Modelling Final Report. A report prepared by Cardno for the Office of Environment and Heritage NSW. Report No. LJ2949/R2745, September 2012, p. 281.

Clauss, G.F., Kühhnlein, W.L., 1997. Simulation of design storm wave conditions with tailored wave groups. The Seventh International Offshore and Polar Engineering Conference. In: https://onepetro.org/ISOPEIOPEC/proceedings-abstract/ISOPE97/All-ISOPE97/ISOPE-I-97-290/23983. ISOPE-I-97-290.

Carley, J.T., Cox, R.J., 2003. A Methodology for Utilising Time-Dependent Beach Erosion Models for Design Events. In: Kench, P., Hume, T. (Eds.), Proceedings of the 16th Australasian Coasts and Ports Conference, 9-12 September 2003. Auckland. New Zealand. Paper No. 28.

Couriel, E., 2021. Wamberal Terminal Coastal Protection Assessment, Stage 4 – Sand Nourishment Investigation. A report prepared by Manly Hydraulics Laboratory and UNSW Water Research Laboratory for Central Coast Council. Report No. MHL2795, December 2021, p. 69.

Cowell, P.J., Roy, P.S., Jones, R.A., 1995. Simulation of large scale coastal change using a morphological behaviour model. Mar. Geol. 126, 45–61. https://doi.org/10.1016/0025-3227(95)00065-7.

Daley, M., 2011. Disequilibrium-Stress Induced Shoreface Evolution. PhD thesis. School of Geosciences, University of Sydney, Australia, p. 340.

Danish Hydraulic Institute [DHI], 2022a. MIKE 21 Spectral Wave Module, Scientific Documentation. DHI Water & Environment, Hørsholm, Denmark.

Danish Hydraulic Institute [DHI], 2022b. MIKE 21 & MIKE 3 Flow Model FM, Hydrodynamic and Transport Module, Scientific Documentation. DHI Water & Environment, Hørsholm, Denmark.

Durrant, T., Greenslade, D., Hemer, M., Trenham, C., 2014. A Global Wave Hindcast focussed on the Central and South Pacific. CAWCR Technical Report No. 070, The Centre for Australian Weather and Climate Research - A partnership between CSIRO and the Bureau of Meteorology, April 2014, p. 34.

Engelund, F., Fredsøe, J., 1976. A sediment transport model for straight alluvial channels. Hydrol. Res. 7, 293–306.

Evans, J.L., Braun, A., 2012. AClimatology of Subtropical Cyclones in the South Atlantic. Journal of Climate 25. https://journals.ametsoc.org/view/journals/clim/25/21/jcli-d-11-00212.1.pdf.

Ferland, M.A., 1990. Shelf Sand Bodies in Southeastern Australia. Unpublished PhD thesis. Department of Geography, University of Sydney, NSW, Australia.

Fredsøe, J., Andersen, O.H., Silberg, S., 1985. Distribution of suspended sediment in large waves. J. Waterw. Port Coast. Ocean Eng. 111 (6), 1041–1059. https://doi.org/10.1061/(ASCE)0733-950X(1985)111:6(1041).

Goda, Y., 2010. Random Seas and Design of Maritime Structures. World Scientific, Singapore, p. 464.

Goodwin, I.D., 2025. Synoptic Paleoclimatology – The Weather Regime Approach form the Tropics to the Poles. Cambridge University Press, p. 756.

Goodwin, I.D., Freeman, R., Blackmore, K., 2013. An insight into headland sand bypassing and wave climate variability from shoreface bathymetric change at Byron Bay, New South Wales, Australia. Mar. Geol. 341, 29–45. https://doi.org/10.1016/j.margeo.2013.05.005.

Goodwin, I.D., Mortlock, T.R., Browning, S., 2016. Tropical and extratropical-origin storm wave types and their influence on the East Australian longshore sand transport system under a changing climate. J. Geophys. Res. Oceans 121, 4833–4853. https://doi.org/10.1002/2016JC011769.

Goodwin, I.D., Ribo, M., Mortlock, T., 2020. Chapter 25: Coastal sediment compartments, wave climate and centennial-scale sediment budget: The south-eastern Australian example. In: Jackson, D., Short, A. (Eds.), Sandy Beach Morphodynamics. Elsevier, pp. 615–640.

Griffin, J.D., Hemer, M.A., Jones, B.G., 2008. Mobility of sediment grain size distributions on a wave dominated continental shelf, southeastern Australia. Mar. Geol. 252 (1–2), 13–23. https://doi.org/10.1016/j.margeo.2008.03.005.

Hallermeier, R.J., 1981. A profile zonation for seasonal sand beaches from wave climate. Coast. Eng. 4, 253–277. https://doi.org/10.1016/0378-3839(80)90022-8.

Harley, M.D., Turner, I.L., Short, A.D., 2015. New insights into embayed beach rotation: the importance of wave exposure and cross-shore processes. J. Geophys. Res. Earth Surf. 120, 1470–1484. https://doi.org/10.1002/2014JF003390.

Harley, M.D., Masselink, G., de Alegria-Arzaburu, A.R., Valiente, N.G., Scott, T., 2022. Single extreme storm sequence can offset decades of shoreline retreat projected to result from sea-level rise. Commun. Earth Environ. 3, 112. https://doi.org/10.1038/s43247-022-00437-2.

Harris, C.K., Wiberg, P., 2002. Across-shelf sediment transport: interactions between suspended sediment and bed sediment. J. Geophys. Res. Oceans 107 (C1). https://doi.org/10.1029/2000JC000634, 8-1-8-12.

Holthuijsen, L.H., Herman, A., Booij, N., 2003. Phase-decoupled refraction–diffraction for spectral wave models. Coast. Eng. 49, 291–305.

Kinsela, M., Daley, M.J.A., Cowell, P.J., 2016. Origins of Holocene coastal strandplains in Southeast Australia: shoreface sand supply driven by disequilibrium morphology. Mar. Geol. 374, 14–30. https://doi.org/10.1016/j.margeo.2016.01.010.

Li, L., 2010. A Fundamental Study of the Morphological Acceleration Factor. Masters thesis. TU Delft, The Netherlands.

Lowe, R.J., Falter, J.L., Bandet, M.D., Pawlak, G., Atkinson, M.J., Monismith, S.G., Koseff, J.R., 2005. Spectral wave dissipation over a barrier reef. J. Geophys. Res. 110 (C04001). https://doi.org/10.1029/2004JC002711.

McCormick, M.I., 1994. Comparison of field methods for measuring surface topography and their associations with a tropical reef fish assemblage. Mar. Ecol. Prog. Ser. 112, 87–94. https://doi.org/10.3354/meps112087.

Mortlock, T.R., Goodwin, I.D., 2015. Directional wave climate and power variability along the Southeast Australian Shelf. Cont. Shelf Res. 98, 36–53. https://doi.org/10.1016/j.csr.2015.02.007.

Mortlock, T.R., Goodwin, I.D., McAneney, K.J., Roche, K., 2017. The June 2016 Australian East Coast Low: importance of wave direction for coastal erosion assessment. Water 9 (2), 121. https://doi.org/10.3390/w9020121.

Nelson, R.C., 1996. Hydraulic roughness of coral reef platforms. Appl. Ocean Res. 18, 265–274. https://doi.org/10.1016/S0141-1187(97)00006-0.

Niedoroda, A.W., Swift, D.J.P., Hopkins, T.S., Ma, C.-M., 1984. Shoreface morphodynamics on wave-dominated coasts. Dev. Sedimentol. 39, 331–354. https://doi.org/10.1016/S0070-4571(08)70153-5.

Nielsen, P., 1992. Coastal Bottom Boundary Layers and Sediment Transport, Advanced Series in Ocean Engineering, 4. World Scientific, Singapore, p. 340.

O'Donoghue, T., Wright, S., 2004. Flow tunnel measurements of velocities and sand flux in oscillatory sheet flow for well-sorted and graded sands. Coast. Eng. 51 (11−12), 1163–1184. https://doi.org/10.1016/j.coastaleng.2004.08.001.

Office of Environment and Heritage (2017), NSW Coastal Erosion Hot Spots. Available online: http://www.environment.nsw.gov.au/coasts/coasthotspots.htm (accessed on 8 August 2017).

Patterson, D.C., Nielsen, P., 2016. Depth, bed slope and wave climate dependence of long term average sand transport across the lower shoreface. Coastal Engineering 117, 113–125. https://doi.org/10.1016/j.coastaleng.2016.07.007.

Pemberton, S.G., MacEachern, J.A., Dashtgard, S.E., Bann, K.L., Gingras, M.K., Zonneveld, J.-P., 2012. Chapter 19 – Shorefaces. In: Dev. Sedimentol, 64, pp. 563–603. https://doi.org/10.1016/B978-0-444-53813-0.00019-8.

Ranasinghe, R., Swinkels, C., Luijendijk, A., Roelvink, D., Bosboom, J., Stive, M., Walstra, D., 2011. Morphodynamic upscaling with the MORFAC approach: dependencies and sensitivities. Coast. Eng. 58 (8), 806–811. https://doi.org/10.1016/j.coastaleng.2011.03.010.

Ribó, M., O'Brien, P., Goodwin, I.D., Mortlock, T.R., 2020. Shelf sand supply determined by glacial-age sea-level modes, submerged coastlines and wave climate. Sci. Rep. 10, 462. https://doi.org/10.1038/s41598-019-57049-8.

Roelvink, J.A., 2006. Coastal morphodynamic evolution techniques. Coast. Eng. 53, 277–287. https://doi.org/10.1016/j.coastaleng.2005.10.015.

Rosati, J.D., 2005. Concepts in sediment budgets. J. Coast. Res. 21, 307–322. https://doi.org/10.2112/02-475A.1.

Rosati, J.D., Dean, R.G., Walton, T.L., 2013. The modified Bruun rule extended for landward transport. Mar. Geol. 340, 71–81. https://doi.org/10.1016/j.margeo.2013.04.018.

Roy, P.S., 1998. Cainozoic geology of the New South Wales coast and shelf. In: Scheibner, E., Basden, H. (Eds.), Geology of New South Wales: Synthesis, Vol. 2

Geological Evolution, 13. Geological Survey of New South Wales Memoir, pp. 361–385.
Roy, P.S., Stephens, A.W., 1980. Regional Geological Studies of the N.S.W. Inner Continental Shelf Summary Results. Geological Survey Report GS 544, 1980/028, Geological Survey of NSW, Department of Mines, Sydney, Australia.
Ruessink, B.G., Michallet, H., Abreu, T., Sancho, F., Van der, D.A., Van der Werf, A.J.J., Silva, P.A., 2011. Observations of velocities, sand concentrations, and fluxes under velocity-asymmetric oscillatory flows. J. Geophys. Res. 116 (C3). https://doi.org/10.1029/2010JC006443.
Saha, S., Moorthi, S., Pan, H.-L., Wu, X., Wang, J., Nadiga, S., Tripp, P., Kistler, R., Woollen, J., Behringer, D., Liu, H., Stokes, D., Grumbine, R., Gayno, G., Wang, J., Hou, Y.-T., Chuang, H.-Y., Juang, H.-M.H., Sela, J., Iredell, M., Treadon, R., Kleist, D., Van Delst, P., Keyser, D., Derber, J., Ek, M., Meng, J., Wei, H., Yang, R., Lord, S., Van Den Dool, H., Kumar, A., Wang, W., Long, C., Chelliah, M., Xue, Y., Huang, B., Schemm, J.-K., Ebisuzaki, W., Lin, R., Xie, P., Chen, M., Zhou, S., Higgins, W., Zou, C.-Z., Liu, Q., Chen, Y., Han, Y., Cucurull, L., Reynolds, R.W., Rutledge, G., Goldberg, M., 2010. The NCEP climate forecast system reanalysis. Bull. Am. Meteorol. Soc. 91 (8), 1015–1057. https://doi.org/10.1175/2010BAMS3001.1.
Shand, T.D., Goodwin, I.D., Mole, M.A., Carley, J.T., Browning, S.A., Coghlan, I., Harley, M.D., Pierson, W.J., 2011. NSW Coastal Inundation Hazards Study: Coastal Storms and Extreme Waves. WRL Technical Report 2010/16. Water Research Laboratory & Climate Futures at Macquarie University, University of New South Wales, p. 75.
Shepherd, T.G., 2019. Storyline approach to the construction of regional climate change information. Proc. R. Soc. A Math. Phys. Eng. Sci. 475, 20190013. https://doi.org/10.1098/rspa.2019.0013.
Shepherd, T.G., 2021. Bringing physical reasoning into statistical practice in climate-change science. Clim. Chang. 169 (2), 1–2. https://doi.org/10.1007/s10584-021-03226-6.
Shepherd, T.G., Boyd, Emily, Calel, Raphael A., Chapman, Sandra C., Dessai, Suraje, Dima-West, Ioana M., Fowler, Hayley J., James, Rachel, Maraun, Douglas, Martius, Olivia, Senior, Catherine A., Sobel, Adam H., Stainforth, David A., Tett, Simon F.B., Trenberth, Kevin E., van den Hurk, Bart J.J.M., Watkins, Nicholas W., Wilby, Robert L., Zenghelis, Dimitri A., 2018. Storylines: an alternative approach to representing uncertainty in physical aspects of climate change. Clim. Chang. 151, 555–571. https://doi.org/10.1007/s10584-018-2317-9.
Silva, A.P., da Silva, G. Viera, da Silva, P. Gomes, Strauss, D., Tomlinson, R., 2025. Extreme storm events drive beach connectivity through headland bypassing. Sci. Total Environ. 971, 179076. https://doi.org/10.1016/j.scitotenv.2025.179076.
Soldevilla, M.J.M., Martín-Hidalgo, M., Negro, V., López-Gutiérrez, J.S., Aberturas, P., 2015. Improvement of theoretical storm characterization for different climate conditions. Coastal Engineering 96, 71–80.
Stopa, J.E., Cheung, K.F., 2014. Intercomparison of wind and wave data from the ECMWF reanalysis interim and the NCEP climate forecast system reanalysis. Ocean Model 75, 65–83. https://doi.org/10.1016/j.ocemod.2013.12.006.
Taljaard, J.J., 1995. Atmospheric Circulation Systems, Synoptic Climatology and Weather Phenomena of South Africa. Department of Environmental Affairs and Tourism, South Africa, Pretoria, South Africa. Report No. 27–32, South African Weather Bureau.
U.S. Army Corps of Engineers, 2012. Part VI: Design of Coastal Project Elements. In: Coastal Engineering Manual, p. 772.
Valiente, N.G., Masselink, G., Scott, T., Conley, D., McCarroll, R.J., 2019. Role of waves and tides on depth of closure and potential for headland bypassing. Mar. Geol. 407, 60–75. https://doi.org/10.1016/j.margeo.2018.10.009.
Vos, K., Harley, M.D., Turner, I.L., Splinter, K.D., 2023. Pacific shoreline erosion and accretion patterns controlled by El Niño/Southern Oscillation. Nat. Geosci. 16, 140–146. https://doi.org/10.1038/s41561-022-01117-8.
Weber, S.L., 1991. Bottom friction for wind sea and swell in extreme depth limited situations. J. Phys. Oceanogr. 21, 149–172. https://doi.org/10.1175/1520-0485(1991)021<0149:BFFWSA>2.0.CO;2.
Whiteway, T.G., 2009. Australian Bathymetry and Topography Grid. Geoscience Australia Report 2009/21. Australian Government, p. 38.
You, Z., Lord, D., 2008. Influence of the El-Nino-Southern Oscillation on NSW Coastal Storm Severity. J. Coast. Res. 24, 203–207. https://doi.org/10.2112/06-0690.1.